J|A|C|S ARTICLES

Published on Web 08/31/2009

Metalloporphycenes: Synthesis and Characterization of (Pentamethylcyclopentadienyl)ruthenium Sitting-Atop and π-Complexes

Luciano Cuesta,[†] Elizabeth Karnas,[†] Vincent M. Lynch,[†] Ping Chen,[‡] Jing Shen,[‡] Karl M. Kadish,*[,‡] Kei Ohkubo,[§] Shunichi Fukuzumi,*[,§] and Jonathan L. Sessler*[,†]

Department of Chemistry & Biochemistry, University Station-A5300, The University of Texas, Austin, Texas 78712-0165, Department of Chemistry, University of Houston, Houston, Texas 77204-5003, and Department of Material and Life Science, Graduate School of Engineering, Osaka University, SORST, Japan Science and Technology Agency (JST), Suita, Osaka 565-0871, Japan

Received July 8, 2009; E-mail: sessler@mail.utexas.edu; kkadish@uh.edu; fukuzumi@chem.eng.osaka-u.ac.jp

Abstract: Unprecedented porphycene complexes, containing a [RuCp*] (Cp*: pentamethylcyclopentadienyl) fragment accommodated in the central N_4 core or directly bonded to the "π-face" of the macrocycle have been prepared and fully characterized, including via single crystal X-ray diffraction analysis. The optical and electrochemical properties of these new families of compounds were examined in detail, revealing fluorescence in the case of the "sitting-atop" complexes for which the lifetime was determined. For both metal (M = Cu, Ni) porphycene derivatives with a "fused" ruthenocene moiety, strong electronic communication was observed through efficient photoinduced electron transfer from the ruthenocene unit to the macrocycle after laser flash photolysis, affording a charge-separated state. This ruthenocene-macrocycle communication was also confirmed by observation of strong spin−spin coupling in the EPR spectra of the one-electron oxidized species; this allowed for calculation of the distance between the two metal centers.

Introduction

Porphycene, the first and also most stable of the nitrogen-in porphyrin isomers, was prepared in 1986 by Vogel and co-workers.[1] Since then, this planar, aromatic macrocycle, formally [18]porphyrin-(2.0.2.0), has attracted enormous attention due to both theoretical interest and exceptional practical utility.[2] Considering the dominant role that metalloporphyrins have played in the development of porphyrin chemistry, it is not surprising that the coordination chemistry of porphycenes has been closely studied, motivated, in part, from a curiosity vis-à-vis their metal complexation characteristics. Unique physical and optical properties, including strong absorptions in the red region of the UV−vis spectrum have made metalloporphycenes appealing molecules for use in biomedical applications and in the design of new materials.[3,4] In fact, these complexes have been investigated in the context of many applications, including catalysis,[5] protein mimicry,[6] material chemistry,[7] and photodynamic therapy.[8] Moreover, metalloporphycenes have been the subject of numerous physiochemical studies due to a multitude of intriguing chemical, optical, electronic, spectro-

[†] The University of Texas.
[‡] University of Houston.
[§] Osaka University.

(1) Vogel, E.; Köcher, M.; Schmickler, H.; Lex, J. *Angew. Chem., Int. Ed. Engl.* **1986**, *25*, 257–259.
(2) (a) Sessler, J. L.; Weghorn, S. J. In *Expanded, Contracted and Isomeric Porphyrins*; Elsevier: Oxford, 1997. (b) Sessler, J. L.; Gebauer, A.; Vogel, E. In *The Porphyrin Handbook*; Kadish, K. M., Smith, K. M., Guilard, R., Eds.; Academic Press: New York, 2000; Vol. 2, pp 3−32. (c) Sánchez-García, D.; Sessler, J. L. *Chem. Soc. Rev.* **2008**, *37*, 215–232.
(3) See refs 2a−2b, and for recent examples:(a) Rachlewicz, K.; Latos-Grazynski, L.; Vogel, E.; Ciunik, Z.; Jerzykiewicz, L. B. *Inorg. Chem.* **2002**, *41*, 1979–1988. (b) Fowler, C. J.; Sessler, J. L.; Lynch, V. M.; Waluk, J.; Gebauer, A.; Lex, J.; Heger, A.; Zuñiga-y-Rivero, F.; Vogel, E. *Chem.—Eur. J.* **2002**, *8*, 3485–3496. (c) Baba, T.; Shimakoshi, H.; Aritome, I.; Hisaeda, Y. *Chem. Lett.* **2004**, *33*, 906–907. (d) Anju, K. S.; Ramakrishnan, S.; Thomas, A. P.; Suresh, Srinivasan, A. *Org. Lett.* **2008**, *10*, 5545–5548.
(4) Stepien, M.; Donnio, B.; Sessler, J. L. *Chem.—Eur. J.* **2007**, *13*, 6853–6863.
(5) (a) Lo, W.-C.; Che, C.-M.; Cheng, K.-F.; Mak, C. W. *Chem. Commun.* **1997**, 1205–1207. (b) Hayashi, T.; Okazaki, K.; Urakawa, N.; Shimakoshi, H.; Sessler, J. L.; Vogel, E.; Hisaeda, Y. *Organometallics* **2001**, *20*, 3074–3078.
(6) (a) Hayashi, T.; Murata, D.; Makino, M.; Sugimoto, H.; Matsuo, T.; Sato, H.; Shiro, Y.; Hisaeda, Y. *Inorg. Chem.* **2006**, *45*, 10530–10536. (b) Matsuo, T.; Ikegami, T. K.; Sato, H.; Hisaeda, Y.; Hayashi, T. *J. Inorg. Biochem.* **2006**, *100*, 1265–1271. (c) Nakashima, H.; Hasegawa, J.-Y.; Nakatsuji, H. *J. Comput. Chem.* **2006**, *27*, 1363–1372. (d) Matsuo, T.; Tsuruta, T.; Maehara, K.; Sato, H.; Shiro, Y.; Hisaeda, Y.; Hayashi, T. *Inorg. Chem.* **2005**, *44*, 9391–9396. (e) Matsuo, T.; Dejima, H.; Hirota, S.; Murata, D.; Sato, H.; Ikegami, T.; Hori, H.; Hisaeda, Y.; Hayashi, T. *J. Am. Chem. Soc.* **2004**, *126*, 16007–16017. (f) Hayashi, T.; Dejima, H.; Matsuo, T.; Hirota, S.; Sato, H.; Murata, D.; Hisaeda, Y. *J. Am. Chem. Soc.* **2002**, *124*, 11226–11227.
(7) (a) Barbe, J.-M.; Richard, P.; Aukauloo, M. A.; Lecomte, C.; Petit, P.; Guilard, R. *J. Chem. Soc., Chem. Commun.* **1994**, 2757–2758. (b) Saoiabi, A.; Maroufi, N.; Laghzizil, A.; Barbe, J.-M.; Guilard, R. *J. Maro. Chim. Heterocycl.* **2005**, *4*, 65–80.
(8) Stocker, J. C.; Cañete, M.; Juarranz, A.; Villanueva, A.; Horobin, R. W.; Borrel, J. I.; Teixidó, J.; Nonell, S. *Curr. Med. Chem.* **2007**, *14*, 997–1026, and references therein.

 10.1021/ja905284d CCC: $40.75

scopic or photochemical properties.[9] Therefore, metalloporphycene studies, which reveal inter alia new metal complexation features, are likely to be of both fundamental interest and potential practical utility.

Recently, we reported an approach that allows for modulation of the inherent optical and electronic properties of certain metalloporphyrins that is based on direct coordination of a $[RuCp^*]^+$ fragment (Cp* = pentamethylcyclopentadienyl) to the π-electron "face" of these porphyrins.[10] The fusion of a $[RuCp^*]^+$ fragment to one or more pyrrolic subunits serves to enhance the ability of the constituent porphyrin macrocycles to act as an electron acceptor. This, in turn, permits photoinduced electron transfer from the $[RuCp^*]^+$ moiety to the ligated porphyrin,[10] even though metalloporphyrins normally act as electron donors rather than acceptors in photoinduced electron-transfer reactions.[11−14] Since metalloporphycenes are reported to be better electron acceptors than the corresponding metalloporphyrins,[15] the fusion of a $[RuCp^*]^+$ fragment to the pyrrole of a metalloporphycene could lead to systems that are even more conducive to photoinduced charge transfer. However, to date, the direct "fusion" of a metallocene complex onto the porphycene π-electron framework has yet to be reported.

We report herein the synthesis and full characterization of a series of metalloporphycene-ruthenocene fused compounds, including their respective X-ray crystal structures, wherein a $[RuCp^*]^+$ fragment is linked to a porphycene core via direct coordination. Femtosecond and nanosecond laser flash photolysis analyses have revealed that photoinduced electron transfer from the ruthenocene moiety (acting as a donor) to the singlet excited state of the associated metalloporphycenes (acting as acceptors) takes place efficiently following photoexcitation. We also report the synthesis, X-ray crystal structure and full characterization of a new class of "sitting-atop" semisandwich complexes derived from metal-free porphycenes wherein the $[RuCp^*]^+$ fragment is accommodated in the N_4 core. To the best of our knowledge, these latter species are without precedence in the porphycene chemistry literature. These compounds and the metalloporphycene-ruthenocene fused complexes were examined by means of cyclic voltammetry, UV−vis spectroelectrochemistry, EPR spectroscopy and laser flash photolysis.

Results and Discussion

Synthesis and Crystal Structures. As depicted in Scheme 1 and detailed in the Experimental Section, $[RuCp^*(NCMe)_3]PF_6$ reacts with the free-base porphycene, affording the series of complexes **1** (see Scheme 1). The new species were isolated in moderate yields as air-stable dark blue solids and characterized by NMR (^1H and ^{13}C) spectroscopy, elemental analysis and mass spectrometry after chromatographic purification.

The structures of **1b** and **1c** were also analyzed by single crystal X-ray diffraction analysis and the resulting solid state structures (shown as ORTEP drawings) are presented in Figure 1. The crystal structures reveal that the $[RuCp^*]^+$ fragment is bound to the macrocycle in an out-of-plane coordination mode, with the metal centers displaced from the plane described by the N_4 core by 0.889 Å and 0.884 Å, respectively. This results in so-called "sitting-atop" complexes. In these complexes, the porphycene macrocycles are clearly distorted, displaying a significant deviation from planarity, with the pyrrolide units tilted up to accommodate the metallic fragment. The ruthenium(IV) ion is bound to the four porphycene nitrogen atoms and the four Ru−N distances are identical within experimental error. The core of the η^5-Cp* ligand is slightly ruffled in **1b** and **1c**, with the methyl groups being visibly twisted up. This observation is rationalized in terms of steric congestion between the β-substituents and the Cp* rings within these complexes. An analysis of the ^1H NMR and ^{13}C NMR spectra of **1a**, and **1c** reveals the expected set of signals for these symmetric compounds; however, pronounced upfield shifts are observed in the proton resonances signals of the Cp* methyl groups (see Experimental Section, Supporting Information), a fact attributed to strong ring currents in the porphycene core. To the extent such a rationale is correct, this result indicates that, in spite of displaying considerable deviation from planarity, the porphycene macrocycle retains its aromatic character upon metalation.

On the basis of charge considerations, the formal oxidation state of the ruthenium center in the family of complexes **1** is +4; therefore these molecules are not only the first examples of ruthenium porphycenes characterized by single crystal X-ray diffraction, they are also the first reported ruthenium porphycenes with a central metal ion in the tetravalent oxidation state. Although Ru(II) and Ru(III) metalloporphycenes (as opposed to the Ru(IV) complexes of general structure **1**) have been previously reported,[16] precise X-ray diffraction-derived structural details were not provided.

The ability of porphycenes to stabilize central metals ions in high oxidation states is already well-recognized, with examples including complexes of Sn(IV),[9e,17] Ge(IV), Mo(V)[18] and osmium(VI).[16a] However, none of these previously reported high

(9) Selected examples: (a) Schlüpmann, J.; Huber, M.; Toporowicz, M.; Plato, M.; Köcher, M.; Vogel, E.; Levanon, H.; Möbius, K. *J. Am. Chem. Soc.* **1990**, *112*, 6463–6471. (b) Waluk, J.; Müller, M.; Swiderek, P.; Köcher, M.; Vogel, E.; Hohlneicher, G.; Michl, J. *J. Am. Chem. Soc.* **1991**, *113*, 5511–5527. (c) Kadish, K. M.; Van Camelbecke, E.; Boulas, P.; D'Souza, F.; Vogel, E.; Kisters, M.; Medforth, C. J.; Smith, K. M. *Inorg. Chem.* **1993**, *32*, 4177–4178. (d) D'Souza, F.; Boulas, P.; Aukauloo, A. M.; Guilard, R.; Kisters, M.; Vogel, E.; Kadish, K. M. *J. Phys. Chem.* **1994**, *98*, 11885–11891. (e) Vogel, E. *J. Heterocycl. Chem.* **1996**, *33*, 1461–1487. (f) Starukhin, A.; Vogel, E.; Waluk, J. *J. Phys. Chem. A* **1998**, *102*, 9999–10006. (g) Steiner, E.; Fowler, P. W. *Org. Biomol. Chem.* **2003**, *1*, 1785–1789. (h) Vdovin, A.; Sepiol, J.; Urbanska, N.; Pietraszkiewicz, M.; Mordzinski, A.; Waluk, J. *J. Am. Chem. Soc.* **2006**, *128*, 2577–2586. (i) Waluk, J. *Acc. Chem. Res.* **2006**, *39*, 945–952. (j) Aoki, K.; Goshima, T.; Kozuka, Y.; Kawamori, Y.; Ono, N.; Hisaeda, Y.; Takagi, H. D.; Inamo, M. *Dalton Trans.* **2009**, 119–125.

(10) Cuesta, L.; Karnas, E.; Lynch, V. M.; Sessler, J. L.; Kajonkijya, W.; Zhu, W.; Zhang, M.; Ou, Z.; Kadish, K. M.; Ohkubo, K.; Fukuzumi, S. *Chem.−Eur. J.* **2008**, *14*, 10206–10210.

(11) (a) Fukuzumi, S.; Imahori, H. In *Electron Transfer in Chemistry*; BalzaniV., Ed.; Wiley-VCH: Weinheim, 2001; Vol. 2, pp 927−975. (b) Fukuzumi, S. *Org. Biomol. Chem.* **2003**, *1*, 609–620. (c) Fukuzumi, S.; Kojima, T. *J. Mater. Chem.* **2008**, *18*, 1427–1439.

(12) Kadish, K. M.; Van-Caemelbecke, E.; Royal, G. In *The Porphyrin Handbook*; Kadish, K. M., Smith, K. M., Guilard, R., Eds.; Academic Press: San Diego, 2000; Vol. 8, p 1.

(13) Gust, D.; Moore, T. A. In *The Porphyrin Handbook*; Kadish, K. M., Smith, K. M., Guilard, R., Eds.; Academic Press: New York, 2000; Vol. 8, p 153.

(14) Protonated porphyrins can act as good electron acceptors, see: (a) Kojima, T.; Nakanishi, R.; Harada, K.; Ohkubo, S.; Yamauchi, S.; Fukuzumi, *Chem.−Eur. J* **2007**, *13*, 8714–8725. (b) Kojima, T.; Honda, T.; Ohkubo, K.; Shiro, M.; Kusukawa, T.; Fukuda, T.; Kobayashi, N.; Fukuzumi, S. *Angew. Chem., Int. Ed.* **2008**, *47*, 6712–6716. (c) Nakanishi, T.; Kojima, T.; Ohkubo, K.; Fukuzumi, S. *J. Am. Chem. Soc.* **2009**, *131*, 577–584.

(15) Bernard, C.; Gisselbrecht, J. P.; Gross, M.; Vogel, E.; Lausmann, M. *Inorg. Chem.* **1994**, *33*, 2393–2401.

(16) See ref 5a and: (a) Li, Z.-Y.; Huang, J.-S.; Che, C.-M.; Chang, C. K. *Inorg. Chem.* **1992**, *31*, 2670–2672. (b) Owara, T.; Abe, M.; Shimakoshi, H.; Hisaeda, Y. *Chem. Lett.* **2008**, *37*, 906–907.

(17) Vogel, E. *Pure Appl. Chem.* **1990**, *62*, 557–564.

(18) Maeda, D.; Shimakoshi, H.; Abe, M.; Hisaeda, Y. *Dalton Trans.* **2009**, 140–145.

Scheme 1. Synthesis of Complexes **1**−**3**

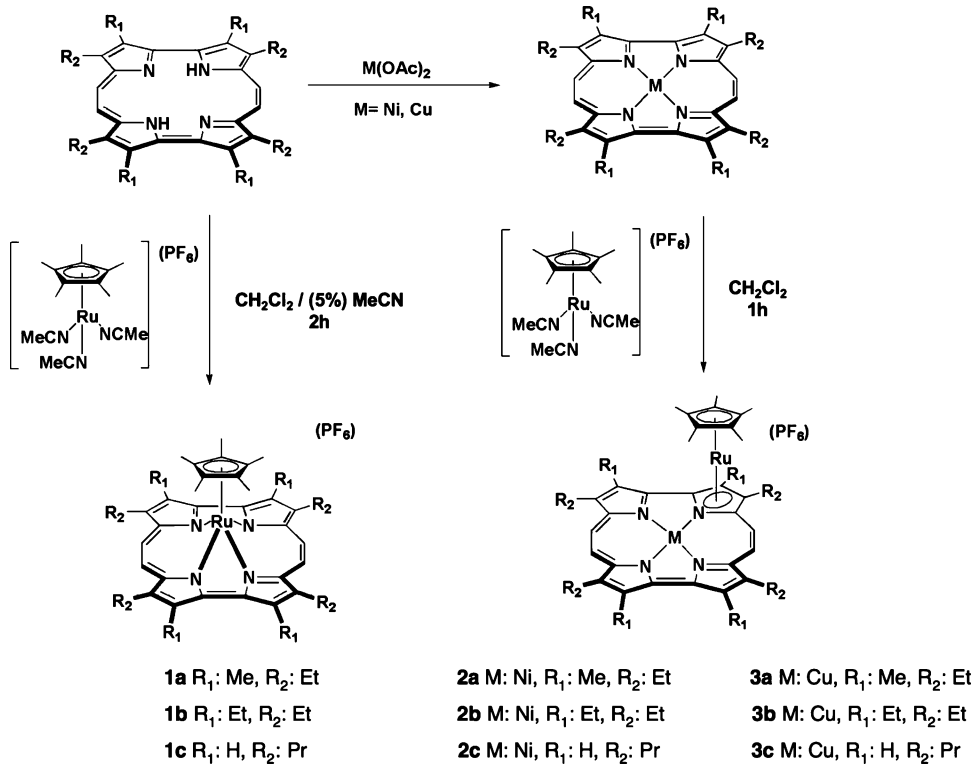

oxidation state metal complexes rely on the use of a η^5-cyclopentadienyl semisandwich coordination mode, as is true in complexes **1a**−**c**. Indeed, we believe these latter species are without precedent, not only in porphycene chemistry, but within

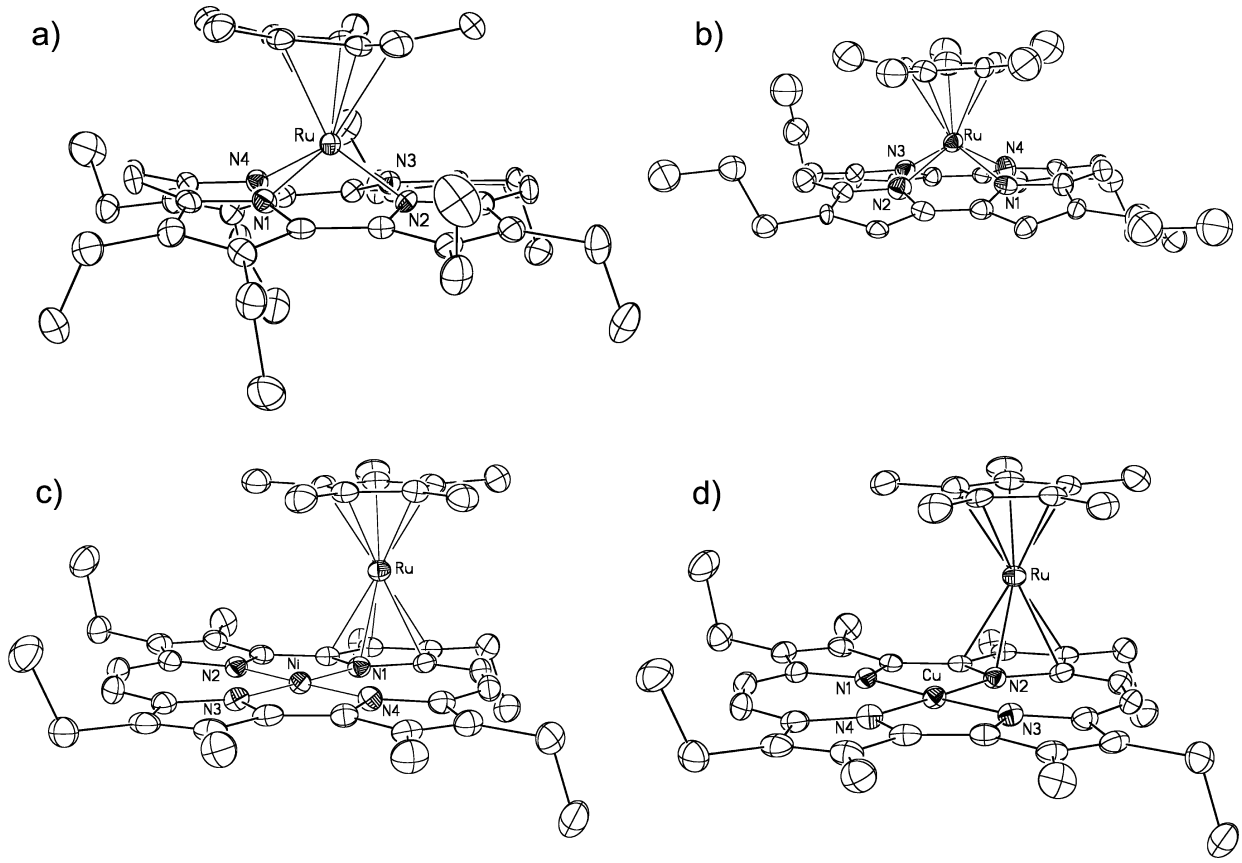

Figure 1. Side views of the complexes **1b** (a), **1c** (b), **2a** (c), and **3a** (d) showing partial atom labeling schemes. Displacement ellipsoids are scaled to the 50% probability level for all complexes. Hydrogen atoms and PF_6 counteranions have been removed for clarity.

the broader context of the porphyrin literature. Our own tests of whether analogous reactions could be carried out with porphyrins failed to afford semisandwich complexes analogous to **1**. While these failures could be attributed to a number of factors, one likely explanation is that the lower flexibility of the porphyrin framework precludes formation of a RuCp*-"sitting-atop" complex. On the other hand, it is important to note that Sc(III)[19] and Zr(III)[20] η^5-cyclopentadienyl semisandwich porphyrin complexes have been prepared; however, they were obtained using a totally different synthetic strategy than was used to obtain the complexes of **1**. Specifically, the electron-deficient nature of early transition metal porphyrin complexes were exploited to effect metathesis reactions involving the axial ligands.

The $[RuCp^*(NCMe)_3]PF_6$ complex also reacts with Ni(II) or Cu(II) metalloporphycenes as shown in Scheme 1. Such reactions yield a family of sandwich complexes **2** and **3** (see Scheme 1), where the ruthenium fragment is directly π-coordinated to one of the pyrrolide subunits so as to produce hybrid "porphycene-ruthenocene" systems. The exceptional ability of this precursor to "coordinate" to the π-surface of the tetrapyrrolic ligand was recently exploited by our group in the case of metallocene-type species based on metalloporphyrins[10] and calix[4]pyrrole,[21] as well as by Rauchfuss and co-workers in the case of phthalocyanines.[22]

The bimetallic complexes **2** and **3** were isolated as dark green solids in good yield after chromatographic purification (see Experimental Section). Both series of complexes are air stable and also relatively stable in noncoordinating solvents, such as CH_2Cl_2. This contrasts to what is seen in coordinating solvents such as MeCN, PhCN or DMSO where competition for binding at the $[RuCp^*]^+$ fragment takes place, leading to a decreased stability of the compound and ultimately dissociation of the ligand.

The bimetallic complexes **2** and **3** were initially characterized using NMR (^1H and ^{13}C) and/or EPR spectroscopy, elemental analysis and mass spectrometry. Single-crystal X-ray diffraction studies of **2a** and **3a** were also carried out (see Figure 1); these latter analyses confirm that a single $[RuCp^*]^+$ fragment is bound to one of the four pyrrolide subunits via π-coordination, while the Ni(II) or Cu(II) ion remains coordinated within the N_4 core of the macrocycle. In contrast to what proved true for complexes of general structure **1**, the macrocyclic rings of **2** and **3** are perfectly planar, with the Cp* ligand being roughly parallel to the mean macrocycle plane. As expected, the central N atom, which is bound to two metal centers (the Ru(II) of $[RuCp^*]^+$ and the Ni(II) or Cu(II) in the macrocycle), displays an elongated N−Ni or N−Cu bond as compared with nitrogen−metal bond distances of similar porphyrin or porphycene macrocycles not having a fused $[RuCp^*]^+$ group.

The loss of symmetry, caused by attachment of the $[RuCp^*]^+$ moiety to one pyrrolide subunit in **2** and **3** is clearly evident in the ^1H and ^{13}C NMR spectra of these compounds, which display the expected number set of signals, including nonequivalent resonances for the β-pyrrolic substituents and the *meso* protons. Particularly revealing is the resonance at 6.61 ppm seen in the ^1H NMR spectrum of **2c**. This signal, a singlet, is attributed to the β-H of the pyrrolide moiety bound to the $[RuCp^*]^+$ fragment. The upfield shift in this resonance relative to the other β-protons is ascribed to the ring current of the Cp* ligand.

The EPR spectra of the compounds **3** all show the characteristic patterns and g values of a Cu(II) porphycene as described in a later section of the manuscript. However, this "normal" Cu(II) porphycene signature is of interest because it arises for a novel set of heterobimetallic complexes, namely **3**, wherein the π-surface of the porphycene has been exploited as a binding site for metallic fragments.

Electrochemistry. The electrochemistry of tetraphenylporphycenes and octaethylporphycenes has been well-characterized in the literature.[9c,d,15,23−25] As is true for porphyrins, these compounds, when dissolved in nonaqueous media, undergo two reversible one-electron reductions and two reversible one electron oxidations, all centered at the conjugated macrocycle, to give π-anion radicals and dianions and π-cation radicals and dications, respectively. Metal-centered one-electron oxidations have also been reported for porphycene derivatives of Ni^{II}, Co^{II} and Ru^{II}, while metal-centered one-electron reductions of the Fe^{III} and Mn^{III} derivatives of porphycene are also known.[9c,d,23−25] Unlike the case of porphyrins, there have been no reports of $Fe^{II/I}$ or $Co^{II/I}$ porphycene reactions, a result best rationalized in terms of the metal(I) ion not being able to fit within the macrocyclic cavity.

The tetrapropylporphycenes are easier to reduce and harder to oxidize than the octaethylporphycenes,[9d,15,25] although the difference in redox potentials between the two series of compounds is not large. Generally, these differences amount to 100 mV or less, with the exact value depending upon the solvent, type of supporting electrolyte and specific central metal ion. Similar electrochemical HOMO−LUMO gaps are observed for compounds in the two series of porphycene macrocycles,[9d,25] with the average value being reported as 1.85 ± 0.15 V. This compares to the 2.25 ± 0.15 V generally observed for most metalloporphyrins[12,13,26] with similar substituents, i.e. compounds in the series of octaethylporphyrins (OEP) and tetraphenylporphyrins (TPP).

The decreased electrochemical HOMO−LUMO gap of metalloporphycenes as compared to metalloporphyrins is due almost exclusively to a change in the LUMO energy and the easier reduction of the porphycene. For example, $(OEPc)Zn^{II}$ is reduced and oxidized at −1.12 and 0.66 V in PhCN[9d] as compared to (OEP)Zn where the same electrode reactions occur at −1.61 and 0.63 V in DMSO.[26] In a similar manner, (OEPc)Cu is reduced and oxidized at −1.05 and 0.83 V in PhCN[9d] as compared to −1.46 and 0.79 V for (OEP)Cu in DMSO.[26]

The metalloporphycenes **1**−**3** in the present paper were initially examined by cyclic voltammetry in both PhCN and CH_2Cl_2 containing 0.1 M TBAP or $TBAPF_6$. Greater complex stability was found for the oxidized and reduced forms in the nonbinding CH_2Cl_2 and this solvent was then used for all further electrochemical measurements. For these studies, $TBAPF_6$ was

(19) Arnold, J.; Hoffman, G. C. *J. Am. Chem. Soc.* **1990**, *112*, 8620–8621.
(20) Kim, H.-J.; Jung, S.; Jeon, Y- M.; Whang, D.; Kim, K. *Chem. Commun.* **1997**, *220*, 2201–2202.
(21) Cuesta, L.; Gross, D.; Lynch, V. M.; Ou, Z.; Kajonkijya, W.; Ohkubo, K.; Fukuzumi, S.; Kadish, K. M.; Sessler, J. L. *J. Am. Chem. Soc.* **2007**, *129*, 11696–11697.
(22) Contakes, S. M.; Beatty, S. T.; Dailey, K. K.; Rauchfuss, T. B.; Fenske, D. *Organometallics* **2000**, *19*, 4767–4774.
(23) D'Souza, F.; Boulas, P. L.; Kisters, M.; Sambrotta, L.; Aukauloo, A. M.; Guilard, R.; Kadish, K. M. *Inorg. Chem.* **1996**, *35*, 5743–5746.
(24) Gisselbrecht, J. P.; Gross, M.; Vogel, E.; Scholz, P.; Broring, M.; Sessler, J. L. *J. Electroanal. Chem.* **2001**, *507*, 244–249.
(25) Gisselbrecht, J. P.; Gross, M.; Koecher, M.; Lausmann, M.; Vogel, E. *J. Am. Chem. Soc.* **1990**, *112*, 8618–8620.
(26) Fuhrhop, J.-H.; Kadish, K. M.; Davis, D. G. *J. Am. Chem. Soc.* **1973**, *95*, 5140–5147.

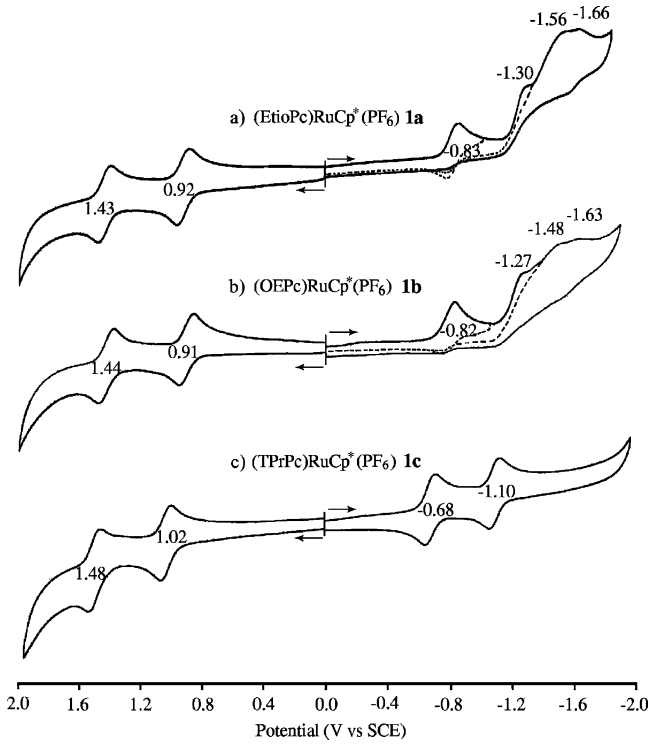

Figure 2. Cyclic voltammograms of compounds **1a**−**c** in CH_2Cl_2 containing 0.1 M $TBAPF_6$.

Table 1. Half-Wave Potentials (V vs SCE) of "Sitting-Atop" Ru Porphycene in Different Solvents Containing 0.1 M $TBAPF_6$

			ox		red		
solvent	temp (K)	cpd	second	first	first	second	HOMO−LUMO gap
CH_2Cl_2	295	**1a**	1.43	0.92	−0.83	−1.30[a,b]	1.75
		1b	1.44	0.91	−0.82	−1.27[a,b]	1.73
		1c	1.48	1.02	−0.68	−1.10	1.70
	203	**1a**	1.34	0.80	−0.89	−1.32	1.69
		1b	1.37	0.86	−0.82	−1.25	1.68
		1c	1.41	0.94	−0.75	−1.15	1.69
PhCN	295	**1b**	1.42	0.91	−0.79[a,b]		1.70

[a] Peak potential at a scan rate of 0.1 V/s. [b] Further reductions involving putative decomposition products are observed.

used as the supporting electrolyte since PF_6^- is less coordinating than ClO_4^-. The UV−vis spectral changes obtained during oxidation and reduction of each complex were also monitored by thin-layer spectroelectrochemistry to determine the stability of the electrogenerated product, the reversibility of the electron addition or abstraction processes, and the probable site of the electron transfer.

Cyclic voltammograms of the three "sitting-atop" complexes in CH_2Cl_2, 0.1 M $TBAPF_6$ were measured at 295 K (Figure 2) and at 203 K (Table 1). Similar potentials were expected for **1a** and **1b** due to the similar macrocycle substituents and this was indeed observed. More difficult oxidations and easier reductions were expected for **1c** and this is also observed (Figure 2c).

The absolute difference in potentials between the first and second one-electron oxidation processes in CH_2Cl_2 range from 460 mV in the case of **1c** to 510 − 530 mV in the case of **1a** and **1b** when 0.1 M $TBAPF_6$ is used as the electrolyte. However, smaller separations are seen for the same compounds in CH_2Cl_2 containing 0.1 M TBAP as the supporting electrolyte. This difference reflects the easier second oxidation, a result which

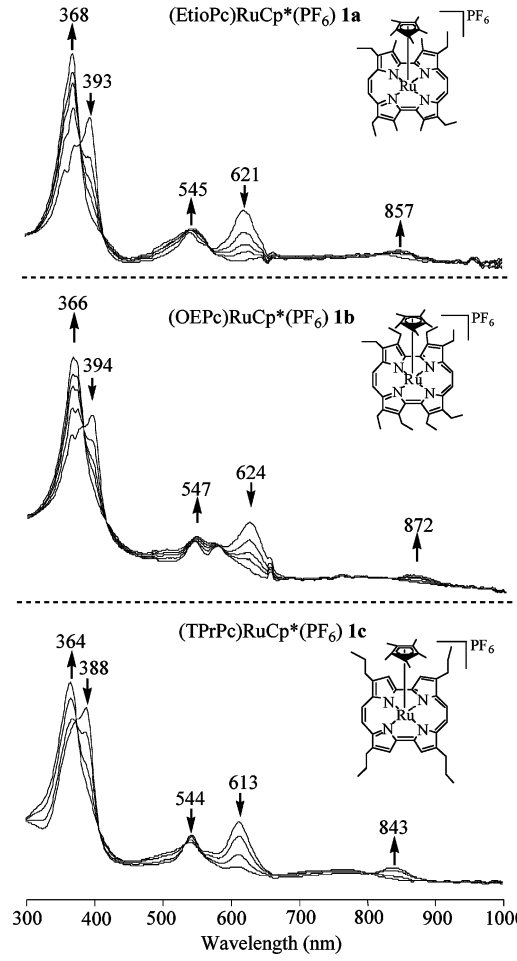

Figure 3. UV−visible spectral changes of **1a**, **1b**, and **1c** observed during the first one-electron oxidation in CH_2Cl_2 containing 0.1 M $TBAPF_6$.

can be ascribed to a stronger association of the doubly oxidized species with the ClO_4^- anion of the supporting electrolyte as compared to PF_6^-. A similar effect was earlier described in the literature for a series of Ni(II) porphyrins.[27]

The Ru center of compounds **1a**−**c** is tetravalent and the two oxidations of these compounds are therefore assigned to ring-centered electron abstractions. UV−vis spectra of the singly oxidized compounds **1a**−**1c** are shown in Figure 3. Inspection of this figure reveals that upon oxidation, these complexes give rise to a broad band in the near-IR region and a decrease in the intensity of the Q-band at 613 to 624 nm, in agreement with the conclusion that the oxidation processes are macrocycle rather than metal centered.

The behavior of the "sitting-atop" complexes is more complicated in the case of reduction. Two reversible one-electron additions are seen at 203 K for all three compounds (see Table 1). The potential separation between the two $E_{1/2}$ values for reduction is about 400 mV, a value slightly larger than the 350−390 mV observed for two one-electron reductions of (OEPc)M and (TPrPc)M, where M are any of a number of divalent transition metal cations under the same solution conditions. There is no evidence for reduction of the Ru(IV) center at low temperature and the two reductions of **1a**−**c** are

(27) Kadish, K. M.; Lin, M.; Van Caemelbecke, E.; De Stefano, G.; Medforth, C. J.; Nurco, D. J.; Nelson, N. Y.; Krattinger, B.; Muzzi, C. M.; Jaquinod, L.; Xu, Y.; Shyr, D. C.; Smith, K. M.; Shelnutt, J. A. *Inorg. Chem.* **2002**, *41*, 6673–6687.

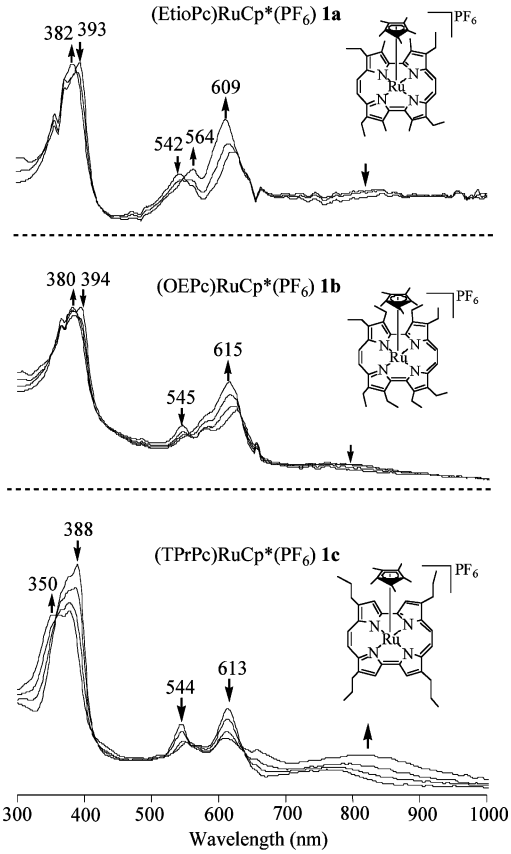

Figure 4. UV−visible spectral changes of **1a**, **1b**, and **1c** observed during the first reduction in CH_2Cl_2 containing 0.1 M $TBAPF_6$ as the supporting electrolyte.

assigned to formation of a π radical anion, followed by formation of the dianion on the cyclic voltammetry time scale.

Interestingly, the spectral changes after the first one-electron reductions are different for **1c** as compared to **1a** and **1b.** Compound **1c** has four β-propyl substituents while **1a** and **1b** have eight β-alkyl substituents. The Soret band of the two complexes with eight alkyl groups (**1a** and **1b**) remains virtually unaffected during the first reduction. In contrast, **1c** shows a loss in Soret band intensity accompanied by appearance of a broad radical signal in the visible region (Figure 4). These results lead us to suggest that two different reduction products are being formed. This conclusion is supported by the cyclic voltammetric data in Figure 2, which shows a reversible reduction of **1c** and a chemical reaction following reduction in the case of **1a** and **1b**. There are also multiple overlapping redox processes at more negative potentials for the latter two compounds. The nature of the chemical reaction following formation of the monoanion of **1b** was elucidated from electrochemical and spectroelectrochemical measurements carried out in PhCN. In this solvent, the chemical reaction is more rapid than in CH_2Cl_2, and the product of the reaction exhibits two well-defined one-electron reductions at −1.39 and −1.81 V (Figure 5).

Controlled potential reduction of **1b** in a thin-layer spectroelectrochemical cell gave a final product with well-defined absorption features at 385 and 617 nm. These observations and the overall spectrum leads us to suggest the formation of $(OEPc)Ru^{II}$ with an unreduced macrocycle. In this context it is noteworthy that the UV−visible spectra of (OEPc)Cu and $(OEPc)Fe^{II}$, which have bands at 395 and 626 nm and at 378

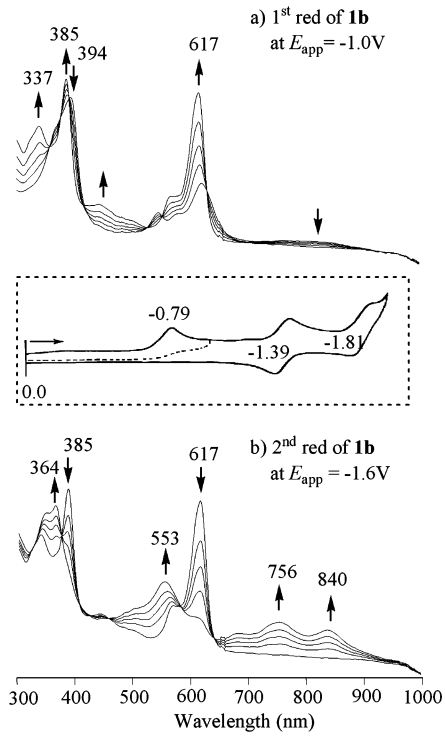

Figure 5. UV−vis spectral changes of $(OEPc)RuCp^*(PF_6)$ **1b** observed during the first and second reductions in PhCN containing 0.2 M $TBAPF_6$ (inset: cyclic voltammogram of reductions).

Scheme 2

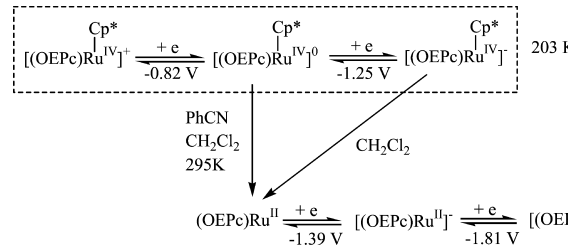

and 623 nm, respectively, are not substantially different than that of $(OEPc)Ru^{II}$.[9d]

A series of singly reduced $(OEPc)M^{II}$ derivatives have been shown to have two near-IR bands at 735−776 and 851−874 nm,[9d] and an identical spectral pattern is seen after the second reduction of $(OEPc)RuCp^*(PF_6)$ in a thin-layer cell. This leads us to suggest that the reduction at −1.39 V involves (OEPc)Ru, a species that is formed as shown in Scheme 2. A further reduction of $[(OEPc)Ru]^-$ to give $[(OEPc)Ru]^{2-}$ then occurs at −1.81 V, as illustrated in Figure 5.

Apparently, the presence of eight versus four alkyl electron-donor groups can sufficiently affect the electronic properties of the "sitting-atop" metalloporphycenes **1**, such that **1c** is more favorably disposed to accept an electron at the π-ring system without loss of the axial ligand. Another aspect related to the presence of eight versus four alkyl groups is the obvious increase in steric repulsion, which can influence the degree of planarity upon coordination. Changes in planarity are known to alter the electrochemistry of porphyrins and related ligands.[9e,17] However, the solid state structures of **1b** and **1c** have been elucidated by X-ray diffraction studies (Figure 1) and comparable deviations from planarity are observed in both cases. In the coordination chemistry of porphycenes, it is well-known that the choice of

Table 2. Half-Wave Potentials (V vs SCE) of Hybrid Ruthenocene-Porphycene Complexes in CH_2Cl_2

		ox		red		
metal	cpd	second	first	first	second	HOMO−LUMO gap
Ni[a]	**2a**		1.11[c]	−0.43	−0.89	1.54
	2b		1.11[c]	−0.42	−0.89	1.53
	2c		1.19[c]	−0.35	−0.80	1.54
Cu[b]	**3a**	1.34	1.06	−0.47	−0.93	1.53
	3b	1.34	1.11	−0.48	−0.96	1.59
	3c	1.35	1.14	−0.38	−0.83	1.52

[a] Containing 0.1 M TBAP as supporting electrolyte. [b] Containing 0.1 M $TBAPF_6$ as supporting electroylte. [c] Peak potential for irreversible reaction. Product of chemical reaction is oxidized at $E_{1/2} = 1.20$ to 1.36 V and reduced at $E_{pc} = 0.79$ to 0.88 V (see Figure 6).

peripherial substituents can play an important role in defining the properties of the final complexes, both for steric and electronic reasons;[2a,9e,17] therefore, it is not surprising, that the electron transfer features can be "altered" as a function of the β-groups present on the porphycene ring.

The hybrid ruthenocene-porphycene systems **2** and **3** were also investigated by cyclic voltammetry and this data is summarized in Table 2. The Ni(II) complexes **2a**, **2b**, and **2c**, unfortunately, decompose after oxidation losing the $[RuCp^*]^+$ fragment, as inferred from the CV and spectroelectrochemistry data. In the case of the three Cu(II) derivatives (**3**), the complexes were stable enough under the electrochemical conditions to display reversible processes, namely, two oxidations located at $E_{1/2} = 1.06$ and 1.34 V for **3a**, 1.11 and 1.34 V for **3b**, and 1.14 and 1.30 V for **3c**. Two reductions are also seen at $E_{1/2} = -0.47$ and −0.93 V for **3a**, −0.48 and −0.96 V for **3b**, and −0.38 and −0.83 V for **3c**. Analysis of these processes by means of thin-layer spectroelectrochemistry was possible (for the reduction, see Figures S39 and S40, Supporting Information), but decomposition of the singly or doubly oxidized species resulted. Based on recently reported data for related porphyrin systems,[10] the first oxidation is assigned to the ruthenium center, an assignment consistent with the EPR data described below. The electrochemical behavior of the sandwich complexes **2** and **3** revealed a considerable difference, specifically a greater ability to accept an electron, when compared with their precursors as seen in Figure 6. This is consistent with the presence of significant electronic communication between the organometallic moiety and the macrocycle.

EPR Spectra. Compounds of general structure **3** are amenable to study by EPR due to the coordinated Cu(II), which has one unpaired electron in its $3d^9$ configuration. The EPR spectrum for **3b** recorded in CH_2Cl_2 at 4 K is shown in Figure 7a together with the computer simulation spectrum (Figure 7b), which allowed us to determine the g and A tensor trace values. Although the EPR spectrum revealed features that are typical for square planar Cu(II) complexes with $d_{x^2-y^2}$ ground state: $g_z > g_x, g_y$, the g and A values are quite different from those for Cu(II) porphyrins.[28−30] First of all there is no axial symmetry: $g_z \neq g_x$, $A_x \neq A_y$, as is expected from the broken symmetry due to the appended $[RuCp^*]^+$. In addition, the g_z value (2.375) is unusually large compared to those of Cu(II) porphyrins (typically 2.189 for (TPP)Cu).[29] The g and A values depend on the energy differences between d orbitals and the g_z value is given by eq 1,

$$g_z = 2.0023 - 8\lambda/\Delta_z \quad (1)$$

where λ, which is inherently negative, is the spin−orbit coupling constant of the free Cu^{2+} ion and $\Delta_z = E(x^2 - y^2) - E(xy)$.[30−33]

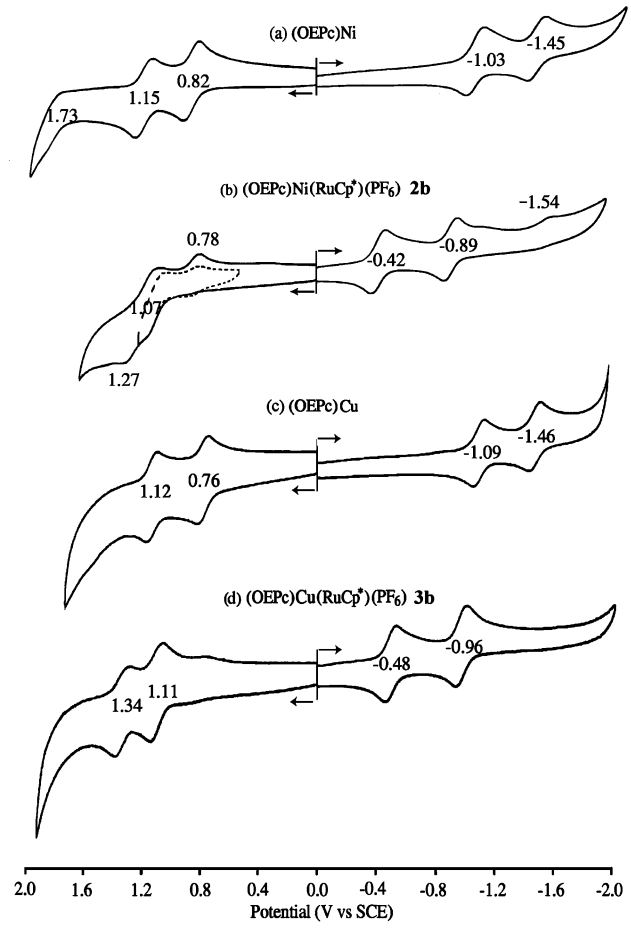

Figure 6. Cyclic voltammograms of (a) (OEPc)Ni, (b) [(OEPc)Ni(RuCp*)]-(PF_6) **2b** (c) (OEPc)Cu and (d) [(OEPc)Cu(RuCp*)](PF_6) **3b** in CH_2Cl_2 containing 0.1 M TBAP.

Thus, the large g_z value results from the small energy gap between $d_{x^2-y^2}$ and d_{xy} as compared with that of Cu(TPP) due to the appended $[RuCp^*]^+$, which increases ionic character of the Cu−N bond of the pyrrolide unit fused to the $[RuCp^*]^+$. The increase in ionic character of the Cu−N bond results in a decrease in the covalent character, leading to a decrease in the Δ_z value. Theoretically the small Δ_z value is expected to decrease the $|A_z|$ value, but to increase the $|A_y|$ value.[33,34] This is why the observed A_y value (110 G) is unusually large compared the A_z and A_x values of 85 and 50 G respectively, whereas normally, Cu(TPP) exhibits a large A_z value (208 G) but small A_x and A_y values (32 G).[29]

The solution EPR spectrum of **3b** recorded at 298 K and the corresponding computer simulation are shown in Figure 7c and Figure 7d, respectively. The isotropic g and A values agree well with the average values of those observed in Figure 7a: $g = (g_x$

(28) Brown, T. G.; Hoffman, B. M. *Mol. Phys.* **1980**, *39*, 1073–1109.
(29) Cunningham, K. L.; McNett, K. M.; Pierce, R. A.; Davis, K. A.; Harris, H. H.; Falck, D. M.; McMillin, D. R. *Inorg. Chem.* **1997**, *36*, 608–613.
(30) Shao, J.; Steene, E.; Hoffman, B. M.; Ghosh, A. *Eur. J. Inorg. Chem.* **2005**, *160*, 9–1615.
(31) Assour, J. M. *J. Chem. Phys.* **1965**, *43*, 2477–2489.
(32) Wertz, J. E.; Bolton, J. R. *Electron Spin Resonance*; Chapman and Hall: New York, 1986; Chapter 11, pp 258−312.
(33) Mabbs, F.; Collison, D. *Studies in Inorganic Chemistry 16: Electron Paramagnetic Resonance of d Transition Metal Compounds*; Elsevier: London, 1992.
(34) A contribution of $3d_{z^2}$ is also important to change the A_x and A_y values. See: Calle, C.; Schweiger, A.; Mitrikas, G. *Inorg. Chem.* **2007**, *46*, 1847–1855.

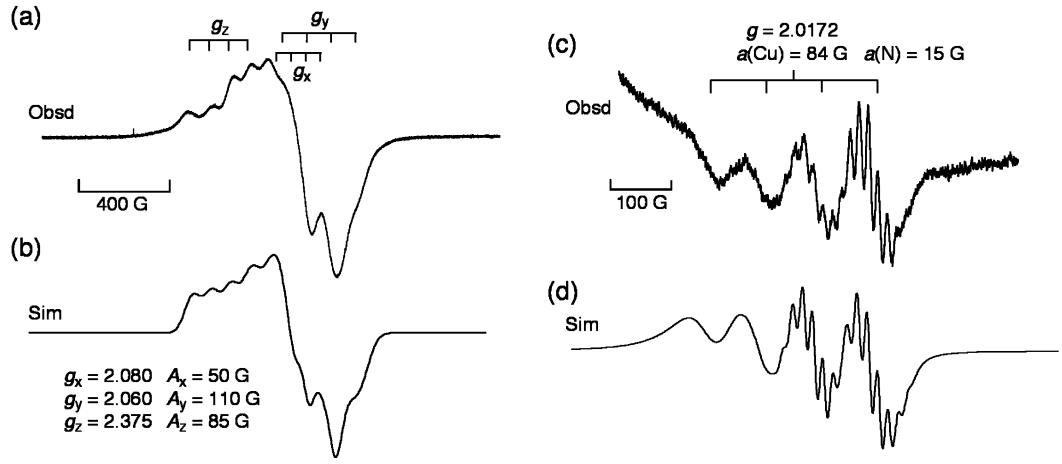

Figure 7. EPR spectra of [(OEPc)Cu(RuCp*)](PF$_6$) (**3b**) in deaerated CH_2Cl_2 (a) at 4 K and (c) at 298 K. (b), (d) Simulated spectra.

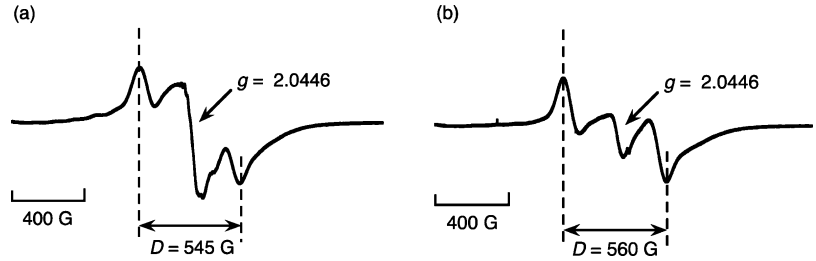

Figure 8. EPR spectra recorded in CH_2Cl_2 at 4 K of (a) [(OEPc)Cu(RuCp*)](PF$_6$) (**3b**) after the addition of 1 equiv of Ru(bpy)$_3^{3+}$ and (b) [(EtioPc)Cu(RuCp*)](PF$_6$) (**3a**) after the addition of 1 equiv of Ru(bpy)$_3^{3+}$.

$+ g_y + g_z)/3$; $a(\mathrm{Cu}) = (A_x + A_y + A_z)$. Such agreement provides support for the EPR parameters determined in Figure 7b. In addition to the hyperfine splitting due to Cu nuclear spin, superhyperfine splitting due to three of four nearly equivalent nitrogens of the ligand is observed at each signal with a different I_z value for the Cu nuclear spin, as seen in Figure 7c. However, it is to be noted that the splittings at higher I_z values ($I_z = 3/2$ and 1/2) are not resolved due to line broadening. This is consistent with the spin density on the nitrogen of the pyrrole fused with [RuCp*]$^+$ being much smaller than that present on the other three pyrrolic nitrogens. Thus, the fusion of a [RuCp*]$^+$ fragment to the pyrroles of Cu(II) porphycenes results in significant change in the EPR parameters. The distribution of the unpaired electron of **3a** was also calculated by DFT methods carried out at the B3LYP/Lanl2DZ level (see Experimental Section, Supporting Information). The SOMO orbital of **3a** is localized on the copper and the four nitrogens of the macrocycle, as shown in Figure S35 (Supporting Information).

Upon subjecting the complex to a one-electron oxidation using Ru(bpy)$_3^{3+}$, a significant change occurs in the EPR spectra, specifically, a pattern characterized by a large spin−spin coupling for the triplet state is observed. These features, which are what would be expected in the case of a Cu(II) and Ru(III) interaction are taken as clear evidence that the first oxidation is centered on the ruthenium center. These results also support the notion that strong electronic communication occurs between the two electroactive fragments. The distance between the two parallel spins could be evaluated from both the *g*-value (2.0446) and the zero-field splitting constant, *D*, at 545 and 560 for **3a** and **3b,** respectively. The calculated distance of 3.70 Å in the case of **3a**, falls within the expected range, considering the observed solid-state Cu−Ru distance for **3a** is 3.612 Å.

Photodynamic Properties. The UV−vis spectra of complexes **1a**−**c** can be considered as "standard", displaying an intense split Soret-like absorption band and two less intense Q-type bands. Porphycene Q-bands are, in general, lower in energy, or red-shifted and more intense as compared to those for porphyrins, and this feature makes porphycenes attractive as potential PDT (photodynamic therapy) agents.[7,35] This difference in spectra is attributed to the difference in symmetry; porphyrins are more symmetrical than their porphycene isomers.[35] While metalation increases the overall symmetry of a porphycene, there is still a symmetry difference between **1a** and **1b**, which both have eight β-alkyl groups and **1c**, which has four β-alkyl groups.

In light of the above considerations, we considered it important to investigate the emissive properties of the "sitting-atop" porphycenes **1a**−**c** when excited at a wavelength that falls within the Q-band region. In fact, both emission and excitation spectra are included in ESI (Figures S2, S5, S8, Supporting Information). Briefly, when **1a** and **1b** are excited at 560 nm, both show two-three peaks between 600 and 700 nm while **1c**, also excited at 560 nm, shows one major peak in this range. As mentioned, porphycenes can display remarkable differences in properties, redox and photophysical, due to small changes in β-substitution, and this disparity is also seen in the case of emissive properties.[36] The quantum yields, Φ_f, for **1a**−**c**, were also investigated, but proved to be too small for accurate determination. Even though the emission is weak, it turned out to be possible, to measure the lifetime of **1a**. Upon irradiation of the Q-type band at 540 nm, the emission was monitored at

(35) Stockert, J. C.; Canete, M.; Juarranz, A.; Villanueva, A.; Horobin, R. W.; Borrell, J. I.; Teixido, J.; Nonell, S. *Curr. Med. Chem.* **2007**, *14*, 997–1026.
(36) Sobolewski, A. L.; Gil, M.; Dobkowski, J.; Waluk, J. *J. Phys. Chem. A* **2009**, *113*, 7714–7716.

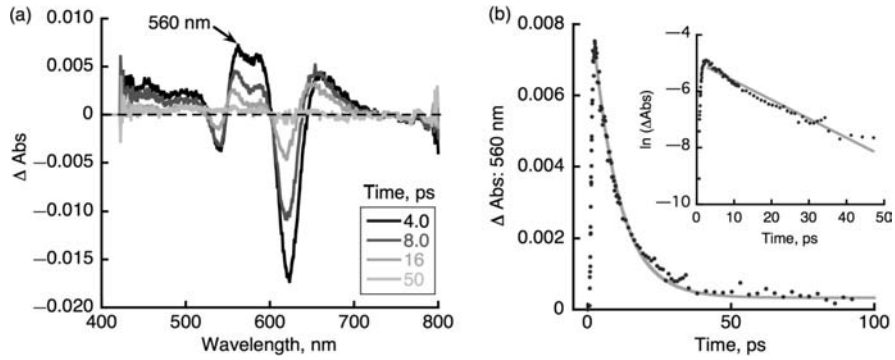

Figure 9. (a) Transient absorption spectra of **1a** in PhCN taken at the indicated times after femtosecond laser pulse irradiation by a 395 nm laser at 298 K. (b) Decay time profile of the absorbance feature at 560 nm with a first-order plot as the inset.

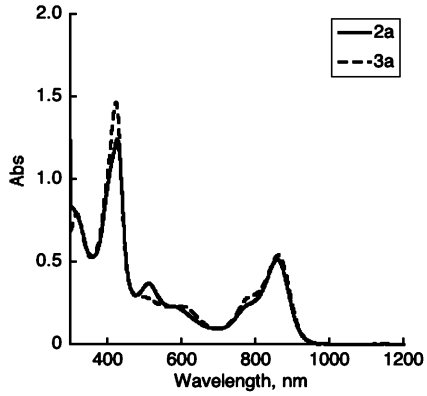

Figure 10. UV−vis spectra of **2a** and **3a** in CH_2Cl_2.

613 nm, and the lifetime was determined to be 4.2 ns (Figure S3, Supporting Information). Femtosecond laser flash photolysis afforded the transient absorption spectra shown in Figure 9a, of which the time profile at 560 nm could be fit to a single exponential decay. This decay process is assigned to an intersystem crossing from the singlet to a triplet excited state with the rate constant, $k_{ISC} = (1.1 \pm 0.03) \times 10^{11}$ s^{-1}.

Unlike the "sitting-atop" complexes, the bimetallic species (**2a**−**c** and **3a**−**c**) display an exceptionally intense broad Q-type band around 870 nm (see Figure 10 for the spectra for the etio-derivatives **2a** and **3a**; see the Supporting Information for the remaining spectra). The presence of these extremely red-shifted bands can be interpreted as another indication of effective electronic communication between the organometallic moieties and the macrocyclic cores. Again, the higher intensity absorption and red shift of the Q-type bands of the porphycenes, when compared with those of porphyrins, make the porphycenes attractive "alternative sensitizers" for PDT,[7,35] an application where functionalization by π-coordination might offer a convenient means for enhancing the photophysical properties of these known macrocycles without the need for new covalent syntheses.

In order to explore further the photophysical properties and the possible internal electronic communications the present complexes might facilitate, femtosecond and nanosecond laser flash photolysis methods (fs lfp, and ns lfp) were employed. The dynamics varied greatly for both the parent compounds in each series, namely Ni-porphycenes vs Cu-porphycenes; they were also seen to vary greatly depending on the nature of the porphycene precursors employed to obtain series **2a**−**2c** and **3a**−**3c**, respectively. To the best of the authors' knowledge, there is no reported transient spectroscopy data for Cu^{II}-porphycenes.

Irradiation of the Soret band for OEPc-Cu(II) (the ruthenium free precursor) at 390 nm by fs lfp shows transient absorption with extremely fast decay, with the rate constant, $k_{ISC} = (5.8 \pm 0.6) \times 10^{10}$ s^{-1} at 480 nm. This can be attributed to an intersystem crossing from the $^2S_1$ (doublet) to the $^2T_1/^4T_1$ (quartet) states due to an expected exchange interaction between an unpaired d_σ electron in Cu(II) and a porphycene π-electron (Figure S29, Supporting Information). Reported lifetimes for this intersystem crossing in the case of Cu(II) porphyrins are on the order of 8 ps or more. This compares well with the OEPc-Cu(II) porphycene on the basis of the above measurements.[37] (Figure S29, Supporting Information) The long-lived-state seen as the remaining absorption at 3000 ps can thus be assigned to the $^4T_1$ state.

In the case of **3b**, transient absorption studies, now with a $[RuCp^*]^+$ fragment fused to the π-electron face of the copper porphycene, revealed the presence of a signal in the NIR region. This broad absorption from 950−1200 nm is proposed to be the CS (charge-separated) state based on spectroelectrochemistry, wherein upon one-electron reduction, a broad absorption to wavelengths extending into the NIR region is seen (Figure S40, Supporting Information). There are clearly two steps that can be fit to a double exponential, and the fit at two separate wavelengths correlate well to one another as can be seen in Figure 11. The first step, involving a fast decay at 500 nm and formation of the absorbance in the NIR region, can be assigned to intramolecular electron transfer (ET) from the ruthenocene moiety to the ring - with the rate constant, $k_{ET} = (3.1 \pm 0.2) \times 10^{10}$ s^{-1}. The second, slower step is attributed to charge recombination (CR), $k_{CR} = (8.8 \pm 0.2) \times 10^8$ s^{-1}, from which a lifetime for the charge-separated state of $\tau = 1.1$ ns is inferred.

Interestingly, features of the transient spectra are similar to those seen in the case of the ruthenocene fused Ni(II) porphycenes, **2a**−**c**, although a much faster decay is observed (Figures S12, S16, S20, Supporting Information). Again, the broad absorption exhibited in the NIR region (Figure 12b), matches that seen in the spectroelectrochemistry experiment for the first reduction of all compounds, **2a**−**2b** (Figure S39, Supporting Information). UV−vis spectra of the one-electron reduced species of **2a** also reveal a slight increase in a broad absorption at 540 and 700 nm (Figure S39, Supporting Information). The parent compound corresponding to **2a**, namely Ni(II)

(37) For a discussion of copper(II) porphyrins and quartet states, see: Asano-Someda, M.; van der Est, A.; Kruger, U.; Stehlik, D.; Kaizu, Y.; Levanon, H. *J. Phys. Chem. A* **1999**, *103*, 6704–6714.

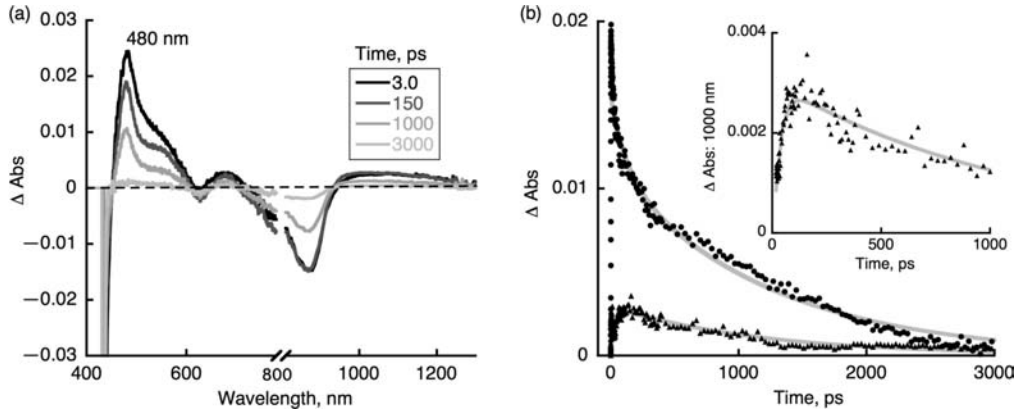

Figure 11. (a) Transient absorption spectra of **3b** in CH_2Cl_2 after femtosecond laser pulse irradiation by a 420 nm laser at 298 K. (b) Decay time profile of the absorbance features at both 500 nm (•) and 1000 nm (▲).

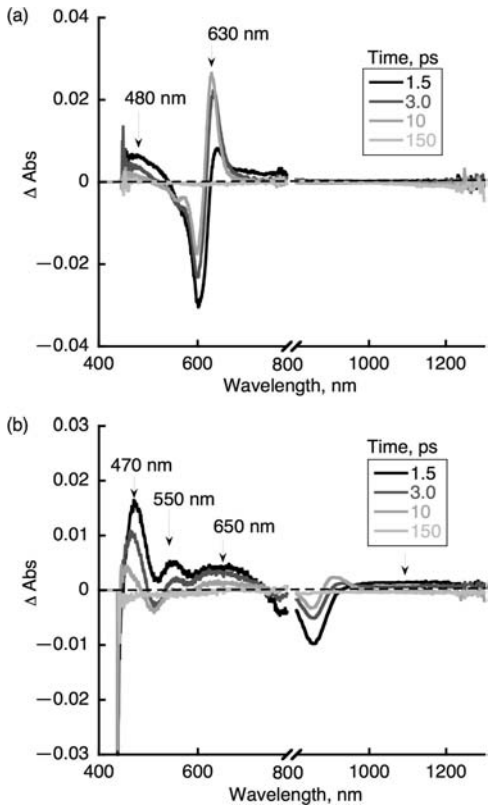

Figure 12. Transient absorption spectra upon femtosecond laser pulse irradiation at 298 K in CH_2Cl_2 of (a) the ruthenium-free Ni(II) porphycene precursor to **2a** (excitation wavelength 390 nm) and (b) complex **2a** (excitation wavelength 420 nm).

porphycene, shows spectral features presumed to be derived from the S_1 excited state, π-localized, with a broad absorption from 450 to 515 nm. These features are subject to bleaching until 630 nm, where a strong positive absorption, with a maximum at 640 nm, is seen. There are no observable absorption features in the NIR region during femtosecond laser excitation of the ruthenium free precursor Ni(II) porphycenes giving rise to **2a**−**c**, as can be seen in Figure 12a, and Figures S17 and S21 (Supporting Information).

Conclusions

In summary, new and unprecedented metalloporphycene complexes, wherein the $[RuCp^*]^+$ fragment is "sitting-atop" the N_4 core or directly coordinated to the π-electron "face" of the macrocycles, have been synthesized. These complexes were characterized by single crystal diffraction analysis, optical spectroscopy, and electrochemical means. The "sitting-atop" complexes containing the metallic fragment bound to the N_4 core exhibit an exceptional electrochemical behavior where the site of electron transfer processes can be "modulated" as a function of the β-pyrrolic substituents. This modulation and indeed the complexes themselves are to the best of the authors' knowledge without precedent in the porphyrin literature.

In the case of the hybrid "ruthenocene-porphycene" complexes, an electronic connection between the $[RuCp^*]^+$ fragment and the π-system of the metalloporphycenes alters the intrinsic electronic properties of the metalloporphycenes in a dramatic way. Specifically, evidence for a very strong interaction between the macrocycle and the "fused" organometallic fragment is seen. This effective communication allows for a photoinduced electron transfer from the ruthenocene unit to the porphycene core, as recently noted in the case of metalloporphyrins.[10] We thus think these systems will be of interest for studying orthogonal π-conjugation effects, wherein coupling of various species above or below the average conjugation plane is used to modulate the inherent aromatic properties of compounds with canonical $4n + 2$ π-electron pathways. In the present instance, where the linkage normal to the aromatic plane involves a redox active species, the resulting modulations in electronics could make the products in question of interest as so-called electron reservoirs or as photodynamic therapy agents with improved optical and excited state properties. Explorations of these possibilities are currently underway.

Acknowledgment. We thank the Fulbright Program and the Spanish Ministry of Education and Science for a postdoctoral fellowship (to L.C.). This work was supported by the National Science Foundation (Grant CHE 0749571 to J.L.S.), a Global COE program, "the Global Education and Research Center for Bio-Environmental Chemistry" from the Ministry of Education, Culture, Sports, Science and Technology, Japan, KOSEF/MEST under the aegis of WCU project (R31-2008-000-10010-0), and the Robert A. Welch Foundation (K.M.K., Grant E-680; J.L.S., F-1018).

Supporting Information Available: Supplementary materials and experimental details. This material is available free of charge via the Internet at http://pubs.acs.org.

JA905284D